Quantum diffusion in spin chains with phase space methods

Jonathan Wurtz* and Anatoli Polkovnikov
Department of Physics, Boston University, 590 Commonwealth Avenue, Boston, Massachusetts 02215, USA

(Received 4 September 2018; revised manuscript received 31 March 2020; accepted 17 April 2020; published 15 May 2020)

Connecting short-time microscopic dynamics with long-time hydrodynamics in strongly correlated quantum systems is one of the outstanding questions. In particular, it is hard to determine various hydrodynamic coefficients such as the diffusion constant or viscosity starting from a microscopic model: exact quantum simulations are limited to either small system sizes or to short times, which are insufficient to reach asymptotic behavior and so various approximations must be applied. We show that these difficulties, at least for particular models, can be circumvented by using the cluster truncated Wigner approximation (CTWA), which maps quantum Hamiltonian dynamics into classical Hamiltonian dynamics in auxiliary high-dimensional phase space. We apply CTWA to *XXZ* next-nearest-neighbor spin-1/2 chains and *XY* spin ladders, and find behavior consisting of short-time spin relaxation which gradually crosses over to emergent diffusive behavior at long times. For a random initial state, we show that CTWA correctly reproduces the whole spin spectral function. Necessary in this construction is sampling from properly fluctuating initial conditions: the Dirac mean-field (variational) ansatz, which neglects such fluctuations, leads to incorrect predictions.

DOI: 10.1103/PhysRevE.101.052120

I. INTRODUCTION

Thermalization of quantum systems has recently become a focus of active research, both theoretical and experimental [1–4]. It has been realized that quantum chaos and emerging relaxation to equilibrium is encoded in the structure of many-body eigenstates of generic quantum Hamiltonians [5–7]. Despite this progress, most theoretical studies of quantum thermalization are either confined to small systems amenable to exact diagonalization [8–11] or to more phenomenological hydrodynamic and kinetic approaches [12–15]. Recently, new approaches such as a novel Gaussian variational approach for quantum impurity systems [16], the time dependent variational principle (TDVP) [17–20], and the cluster truncated Wigner approximation (CTWA) [21] were proposed as viable tools for studying long-time relaxation of quantum systems to thermal equilibrium. The latter two approaches share a common feature that they approximate long-time quantum dynamics with effective nonlinear classical dynamics in a high-dimensional phase space, which can be systematically increased to ensure convergence of the results to the correct ones. This mapping reduces the complexity of the simulations of quantum dynamics from exponential to polynomial in the system size, which should be intuitively sufficient for a proper description of long-time large-scale hydrodynamic behavior. One key feature of the CTWA approach is that unlike mean-field approaches, it contains fluctuating initial conditions distributed according to the appropriate (Wigner) function describing the initial state. Therefore, the information about observables and correlations in CTWA can only be obtained through averaging over many trajectories, each describing a different effective mean-field evolution.

Microscopically, hydrodynamic coefficients can be expressed through appropriate nonequal time correlation functions. In equilibrium, there are various thermodynamic relations between transport and response coefficients such as the fluctuation-dissipation relation [22], drift-diffusion Einstein and Onsager relations [23], and others. These thermodynamic identities imply that a proper formalism describing thermalization should not only explain the relaxation of various observables to their thermal values, but also proper asymptotic behavior of nonequal time correlation functions and the dynamic structure factor $S(k, \omega)$.

In this work, using phase space methods developed previously [21], we study $S(k, \omega)$ for spin-1/2 next-nearest-neighbor *XXZ* chains and *XY* ladders at infinite temperature. In particular, we correctly recover both its high- and low-frequency asymptotics: low frequencies correspond to hydrodynamic diffusive relaxation, while high frequencies describe short-time coherent quantum excitations. These methods smoothly interpolate between the two asymptotic regimes. While high-frequency behavior can be obtained using exact diagonalization in relatively small systems, the correct description of low frequencies for such interacting thermal models requires access to system sizes which are beyond the range of existing methods. We also show that noise in initial conditions is crucial for correctly predicting the structure factor and the spin diffusion constant: cluster mean-field dynamics, obtained from CTWA by suppressing noise, leads to incorrect predictions for subextensive cluster sizes.

II. METHODS

The cluster truncated Wigner approximation (CTWA), introduced in Ref. [21], is the specific phase space method used

*Corresponding author: jwurtz@bu.edu

in this work. The CTWA amounts to first splitting a system of interest into disconnected clusters of spins (labeled "i") and interpreting the complete set of Hermitian operators inside each cluster $G = \{\hat{X}^i_\alpha\}$ as classical phase space variables x^i_α (see Appendix A for details). Quantum operators, including the observables and the Hamiltonian, are mapped to functions of these variables. To describe the dynamics of the system, an ensemble of points is independently evolved in time according to a nonlinear classical Hamiltonian induced from the quantum Hamiltonian, with the initial conditions drawn from a Gaussian probability distribution reproducing averages and fluctuations of the operators $\hat{X}^i_\alpha$ in the initial state. To compute time-dependent expectation values of observables at time t (or, similarly, the nonequal time correlation functions), we average the corresponding functions evaluated on this ensemble of classical trajectories. This sampling of initial conditions is critical: because the dynamics are nonlinear, nearby trajectories generically diverge in time in a way which approximately encodes intercluster correlations and entanglement via correlations in phase space. If all fluctuations are suppressed to zero and a single trajectory is used, then the CTWA reduces to the cluster Dirac mean-field (variational) approximation [24,25].

The CTWA is approximate but improves as the cluster size, and thus the dimensionality of the phase space, increases. This is because the method treats the dynamics within a cluster exactly: it captures all intracluster entanglement and correlations within the expanded phase space. Dynamics between clusters are nonlinear and do not capture any quantum correlations per point in phase space: in this way, the time evolution of the individual points is the mean-field projective dynamics. This means that in the limit of the cluster size to the system size, the method recovers the exact result, with the caveat that the phase space dimensionality is now exponential in the system size (see Appendix A for details). Confidence thus resides in convergence with cluster size, which may be subextensive. The computational difficulty scales as 2^{L+1} in the cluster size, e.g., evolution of wave functions.

One of the quantities that the CTWA can approximately reproduce is the infinite-temperature symmetric nonequal time correlation function of two spin operators $\hat{A}$ and $\hat{B}$,

$$G_{AB}(t,t') = \frac{1}{\mathcal{D}}\mathrm{Tr}[\hat{A}(t)\hat{B}(t')] = \frac{1}{2\mathcal{D}}\mathrm{Tr}[\{\hat{A}(t),\hat{B}(t')\}_+] \equiv \frac{1}{2\mathcal{D}}\sum_n \langle\psi_n|\hat{A}(t)\hat{B}(t') + \hat{B}(t')\hat{A}(t)|\psi_n\rangle, \quad (1)$$

where $\mathcal{D}$ is the total Hilbert space dimension and $\{|\psi_n\rangle\}$ is a complete basis of states. For computational purposes, we sample the correlation function over spin states randomly polarized along the Z axis. Under the CTWA, the expectation value appearing in the equation above for each of the states $|\psi_n\rangle$ is approximately reproduced as

$$\langle\psi_n|\{\hat{A}(t),\hat{B}(t')\}_+|\psi_n\rangle \approx 2\overline{A[\vec{x}(t)]B[\vec{x}(t')]}, \quad (2)$$

where $\vec{x}(t)$ denote coordinates of a specific phase space point evolved to time t drawn from the initial probability distribution, and $A[\vec{x}(t)]$ is the Weyl symbol of the operator $\hat{A}$ evaluated at $\vec{x}(t)$. The overline denotes averaging with respect to Gaussian initial conditions at $t = 0$ corresponding to the state $|\psi_n\rangle$ (see Appendix A and Ref. [21] for details).

III. RESULTS

To demonstrate how the method works, we choose a particular next-nearest-neighbor spin-1/2 XXZ model with periodic boundary conditions, which conserves the total Z magnetization but has no extensive symmetries,

$$\hat{H} = \sum_i^N \hat{\sigma}^i_x\hat{\sigma}^{i+1}_x + \hat{\sigma}^i_y\hat{\sigma}^{i+1}_y + \Delta\hat{\sigma}^i_z\hat{\sigma}^{i+1}_z + \gamma\sum_i^N \hat{\sigma}^i_x\hat{\sigma}^{i+2}_x + \hat{\sigma}^i_y\hat{\sigma}^{i+2}_y + \Delta\hat{\sigma}^i_z\hat{\sigma}^{i+2}_z. \quad (3)$$

Here, $\hat{\sigma}$ represent Pauli matrices. We choose parameters $\Delta = 2$ and $\gamma = 1/2$; for $\gamma = 0$, the model is integrable but still exhibits diffusive behavior [26–28] (see Sec. III A for details).

In Fig. 1, we show the two-time spin-spin correlations $\mathrm{Tr}[\hat{\sigma}^i_\alpha(t)\hat{\sigma}^i_\alpha(t')]/\mathcal{D}$ for $\alpha \in \{x, y, z\}$ as a function of t at dif-

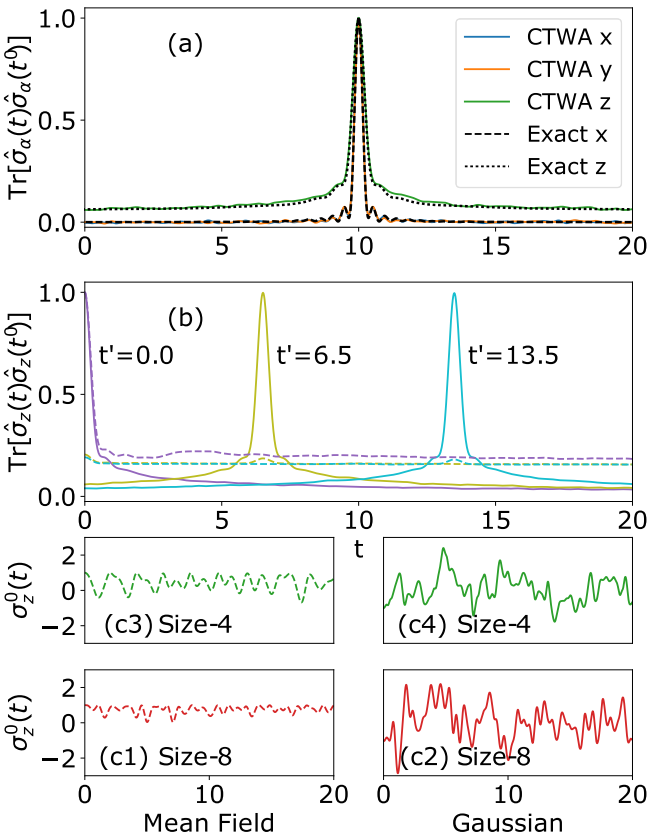

FIG. 1. Nonequal time spin-spin correlation functions of the next-nearest-neighbor XXZ chain of Eq. (3) at infinite temperature. (a) Correlation function for $t' = 10$, compared to exact results; $(L, N) = (8, 16)$. (b) Correlation function for $(L, N) = (8, 64)$, which shows that the correlation function is well captured for offsets t'. The mean field (dashed line) does not capture correctly, emphasizing the importance of fluctuations. (c) Time traces of individual points in phase space for a typical (dashed line) mean-field and (solid line) Gaussian initial condition, and 64 sites. Fluctuations persist at all times for the Gaussian case, but are exponentially small in the cluster size for the mean-field case.

ferent t', initialized in the randomly polarized Z states at $t = 0$. In Fig. 1(a), we use a system size $N = 16$ allowing us to benchmark CTWA with simple exact results: it is clear that the dynamics are almost indistinguishable. This behavior persists at all offsets t', as shown in Fig. 1(b), and is symmetric about $|t - t'|$ as is expected. The mean-field result (colored dashed lines) does not generally reproduce the correlator, emphasizing that the initial noise is critical for the formalism. This time translation invariance is highly nontrivial, as traditional TWA methods usually break down at long times due to divergent ultraviolet noise in the system leading to spurious long-time vacuum heating [29]. On the contrary, within CTWA, quantum noise introduced by the initial Wigner function has a correct scaling with increasing cluster size [21] and persists as a function of time: each point in phase space is generically nonstationary, as is seen in Figs. 1(c2) and 1(c4). This, too, is nontrivial as initial conditions inject an amount of noise exponential in the cluster size L: each point is, on average, a distance $2^{L/2}$ from the mean. This is matched by the exponential size of the phase space, $\sim 4^L$. For the mean field, the noise is only from thermal fluctuations; in particular, it is equal to zero for each initial spin configuration [each $|\psi_n\rangle$ in Eq. (2)]. In turn, in generic ergodic systems, such mean-field trajectories lead to the relaxation of local observables to near constant (thermal) values with exponentially small fluctuations in the cluster size [7] [see Figs. 1(c1) and 1(c3)].

We point out that while the $\sigma_x\sigma_x$ and $\sigma_y\sigma_y$ time correlations decay to zero, the $\sigma_z\sigma_z$ correlation functions decay to a nonzero constant scaling as the inverse system size: $\mathrm{Tr}[\hat{\sigma}_z^i(t)\hat{\sigma}_z^i(t')]/\mathcal{D} \to 1/N$ for $|t - t'| \to \infty$. This result follows from conservation of the total z magnetization: for a typical random initial state, the magnetization scales as $\sqrt{N}$ such that the average magnetization per spin is $1/\sqrt{N}$. Within the mean field, different clusters cannot exchange Z magnetization and thus the spin-spin correlation spuriously relaxes to a higher constant $1/L$ instead of $1/N$, as is seen in Fig. 1(b).

Diffusion of conserved quantities at $\beta = 0$ can be found using the symmetric correlator [30–32], where instead of the particle number we use the (conserved) Z magnetization,

$$C_X(t) = \frac{1}{\mathcal{D}N}\sum_i \mathrm{Tr}\left[\hat{\sigma}_z^i(t)\hat{\sigma}_z^{(i+X)\%N}(0)\right]. \tag{4}$$

For diffusive systems, this correlator should be well approximated by a Gaussian whose width grows in time as $\sqrt{Dt}$, where D is the diffusion constant. Therefore, a natural way to extract the diffusion constant is to compute the width of this correlation as a function of time,

$$R^2(t) = \frac{\sum_X \frac{N^2}{\pi^2}\sin^2\left(\frac{\pi X}{N}\right)C_X(t)}{\sum_X C_X(t)}, \tag{5}$$

and fit it to the solution of the classical diffusion equation (see Appendix C for derivation),

$$R^2(t) = \frac{N^2}{2\pi^2}(1 - e^{-4Dt\pi^2/N^2}). \tag{6}$$

Note that in finite periodic chain systems, we find it more convenient to use this conformal distance between spins; in the limit $N \to \infty$, we recover the typical Gaussian width as, e.g., used in Ref. [32].

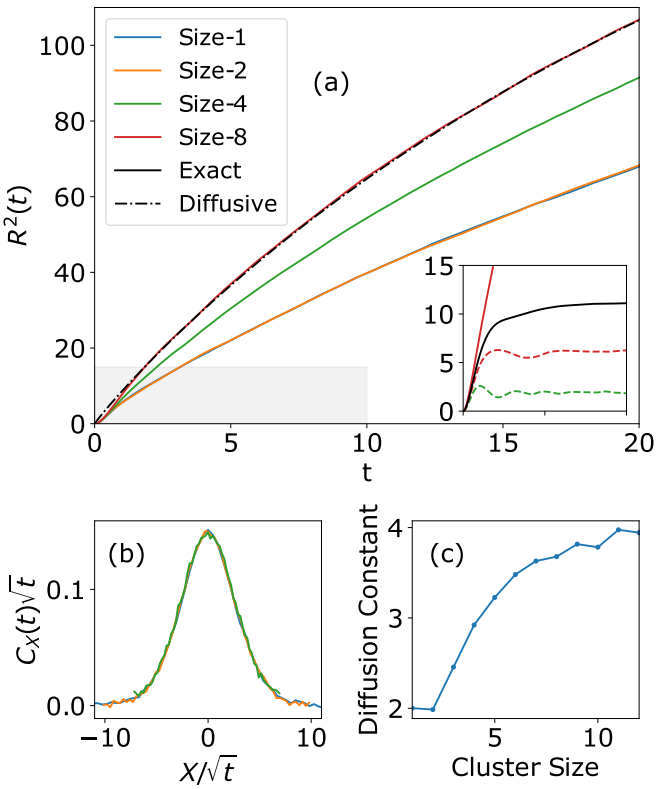

FIG. 2. Diffusive dynamics for the next-nearest-neighbor XXZ chain of Eq. (3) at infinite temperature. (a) The conformal width of the correlation function defined by Eq. (5). The black dashed line is a single-parameter fit for the classical diffusion of Eq. (6). The gray box and inset show a comparison of the exact results for $N = 16$ (solid black line) with CTWA (red solid line) and mean-field (dashed lines) simulations for a larger system $N = 64$. (b) Scaled values of C_X for size-8 clusters, averaged over offsets, which collapses to the form of a Gaussian. Colors are for times $t \in (5, 10, 20)$. (c) A fit of the diffusion constant as a function of cluster size for $N \approx 64$.

In Fig. 2(a), we show the results of numerical simulations of $R^2(t)$ for different cluster sizes and the total system size $N = 64$. Except for short times, all of the curves are well fit by the diffusion prediction (6), although with a cluster-dependent diffusion constant, which saturates with increasing cluster size [Fig. 2(c)] to the asymptotic value $D \approx 3.75$. The inset shows the result of exact evolution for a smaller system size $N = 16$ (CTWA for the same system size will be nearly identical; cf. Fig. 1). It is clear that the system size $N = 16$ is insufficient to see diffusive behavior in this system. Figure 2(b) shows the correlation function $C_X(t)$ rescaled by $\sqrt{t}$ with a very good collapse to the expected Gaussian profile.

For size-1 clusters, the Gaussian profile is expected, as the dynamics of the system is then identical to that of a classical spin chain, which is known to exhibit diffusive behavior over a wide range of parameters [33,34]. However, for larger cluster sizes, the emergent diffusive profile is somewhat nontrivial, as the classical phase space is much larger than the naive one, encoding many "quantum" correlations.

Moreover, dependence of the diffusion constant on the cluster size L [Fig. 2(c)] indicates that it is strongly renormalized by the underlying quantum fluctuations. As in Fig. 1,

we see that the mean-field dynamics [dashed lines in the inset of Fig. 2(a)] is not adequate for correctly capturing long-time diffusive behavior even for relatively large cluster sizes.

Having analyzed the diffusive spreading of correlations, we now move on to study the dynamic structure factor $S(k,\omega)$ and its momentum average $S(\omega)$, containing more complete information about nonequal time spin-spin correlations,

$$S(k,\omega) = \sum_X \int_{-\infty}^{\infty} dt e^{i\omega t + ikX} C_X(t), \tag{7}$$

$$S(\omega) = \frac{1}{N}\sum_k S(k,\omega) = \frac{2\pi}{N}\int_{-\infty}^{\infty} dt e^{i\omega t} C_0(t)$$

$$= \frac{2\pi}{\mathcal{D}} \sum_{mm'} |\langle m'|\hat{\sigma}_z|m\rangle|^2 \delta(\omega - E_m + E'_m). \tag{8}$$

In finite-size quantum systems [35], $S(\omega)$, strictly speaking, consists of isolated δ-function peaks corresponding to discrete energy levels. However, as the number of states exponentially increases with the system size, $S(\omega)$ effectively becomes continuous if we introduce a tiny damping factor into the time integral. We also comment that $S(k=0,\omega=0)$ diverges due to conservation of the total spin $\hat{\sigma}_z$, but this divergence does not play a role at finite frequencies.

Figure 3(a) shows the time correlations at the same site, which, after short-time quantum behavior, decays diffusively as $1/\sqrt{t}$ before saturating at $1/N$. Figure 3(b) shows $S(\omega)$, which is the Fourier transform of Fig. 3(a). It shows that at high frequencies, the structure factor $S(\omega)$ agrees well with exact-diagonalization predictions; the exponential decay as seen here is expected on general grounds [7]. However, the simple exact-diagonalization calculation fails to capture the small frequency diffusive asymptote of the structure factor $S(\omega) \propto 1/\sqrt{\omega}$ [36] due to small system sizes: there is a saturation for $S(\omega < t_c^{-1}) = t_c^{1/2}$, where $t_c \sim N^2$ is the Thouless time [37]. Conversely, CTWA clearly reproduces this asymptote because one can access much larger system sizes. At intermediate frequencies, there is a smooth link between the quantum and classical behaviors, allowing for a correct behavior at all ω. Figures 3(c1)–3(c6) show the dynamic structure factor $S(k,\omega)$ for the first few wave numbers k. Small k represent long length scales where hydrodynamic behavior should dominate. As wavelength increases, the diffusive behavior becomes sensitive to the finite system size, seen as the low-frequency asymptote in both quantum and effective classical dynamics [Figs. 3(c4)–3(c6)]. However, for larger frequencies, the CTWA remains sensitive to smaller length scale effects, with a generic exponential decay in frequency diverging from the $1/\omega^2$ of classical hydrodynamics. Nongeneric behavior in this regime should be well captured simply by exact diagonalization (ED) or, equivalently, intracluster dynamics.

A. Integrable XXZ model

A similar model which shows diffusion despite being integrable is the XXZ model [38], which is described by Eq. (3) for $\gamma = 0$ and $|\Delta| > 1$. The various behaviors of this model have been well studied. In particular, for $\Delta = 0$, it is the XY model, with a mapping to free fermions. For $|\Delta| < 1$, the model is ballistic, and at $\Delta = 1$, it is the Heisenberg model,

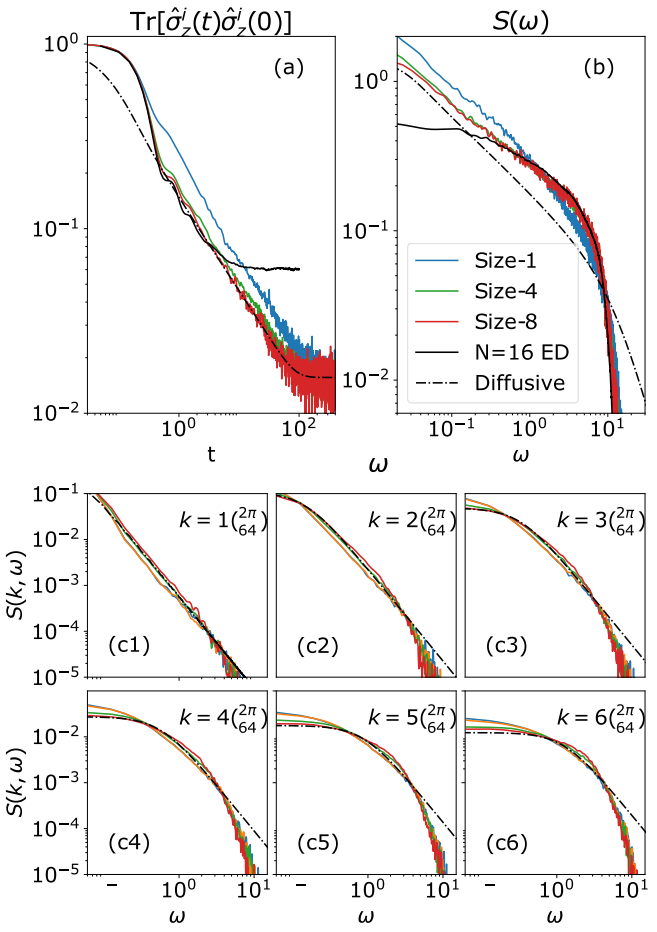

FIG. 3. Dynamic structure factors of the next-nearest-neighbor XXZ chain of Eq. (3) at infinite temperature. (a) Log-log version of Fig. 1(a) showing diffusive decay. (b) Momentum-averaged structure factor $S(\omega)$, which is the Fourier transform of (a). (c1)–(c6) Dynamic structure factor $S(k,\omega)$ for the first few k. The system size is $N = 64$; the dashed black lines are for classical diffusion for $D = 3.75$.

with superdiffusive behavior [14] with exponent $t^{-2/3}$. For $|\Delta| > 1$, the model is diffusive.

This diffusive behavior has been well studied, especially within three contexts: boundary wall quenches, [14,27], nonequilibrium steady states [26,39], and, more recently, from generalized hydrodynamics (GHD) [15,40]. However, the diffusion constant derived from $S(k,\omega)$ does not necessarily need to match that of a quench: the former averages over equilibrium, while the latter studies particular special initial states. It is relatively simple to study both approaches within the CTWA.

Diffusion from $S(k,\omega)$. In Fig. 4, we plot the results of simulations on the 64-site XXZ chain derived from $S(k,\omega)$ and see behavior as expected. For $\Delta < 1$, the model is ballistic: fitting to diffusion does not make sense, although at late times the method will always show diffusive behavior. This is flagged by a nonconvergence in cluster size, which is especially clear for $\Delta = 0$, where the "diffusion constant" fit diverges linearly with cluster size. However, for larger Δ, the diffusion constant does relatively converge with cluster size; for $\Delta = 2$, we find $D \approx 1.2$, an increase of about 1.5 from "classical" size-1 clusters. We find that the diffusion

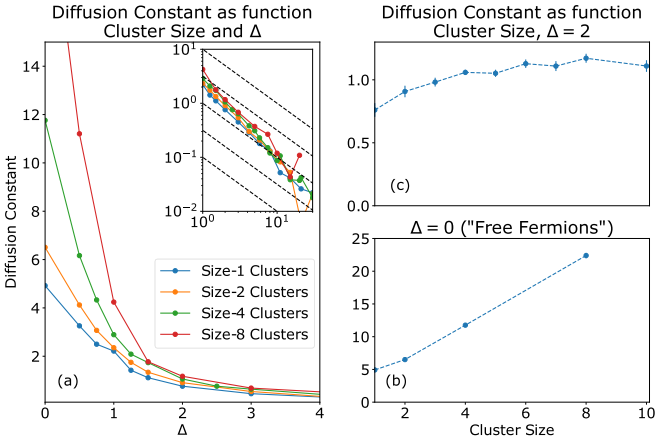

FIG. 4. Diffusion constant for the *XXZ* model as derived from $S(k,\omega)$. (a): Diffusion constant as a function of anisotropy Δ and cluster size. The inset is log-log of the same, showing $1/\Delta$, which is consistent with previous results [30]. Clearly, for $\Delta < 1$, the diffusion constant does not converge, as expected for ballistic behavior (b), while for $\Delta = 2$, it converges to about $1.5\times$ its "classical" value (c).

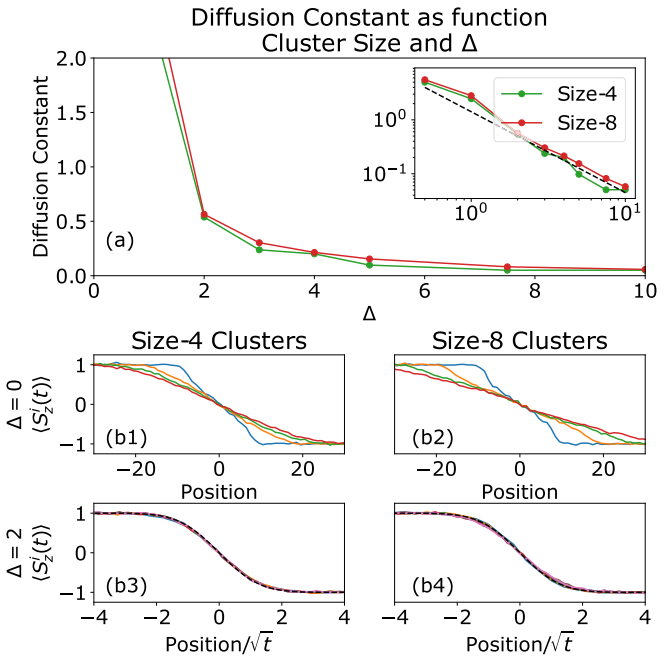

FIG. 5. Diffusion constant for the *XXZ* model as derived from the boundary wall initial condition. (a): Diffusion constant as a function of Δ. For $\Delta < 1$, the diffusion constant diverges, consistent with being nondiffusive. The inset is log-log of the same data; the dashed line is of $\Delta^{-1.5}$. (b1), (b2): Spin profile for $\Delta = 0$, showing ballistic growth improving with cluster size. Lines are for times [2.5,5,7.5,10]. (b3), (b4): Spin profile for $\Delta = 2$, renormalized by $\sqrt{t}$ showing diffusive collapse. The dashed line is the classical profile for $D = 0.52$.

constant scales as Δ^{-1} at large Δ. This finding is consistent with earlier work [30], but potentially inconsistent with more recent work, which predicts $D = 1/3\pi$ for $\Delta \to \infty$ [41] using GHD methods.

Diffusion from a boundary wall. Instead of an infinite temperature state, we study the $\langle S_z(t)\rangle$ dynamics of a boundary quench from an initial pure state, $|\psi\rangle = |\uparrow \ldots \uparrow\uparrow\downarrow\downarrow \ldots \downarrow\rangle$. The results are shown in Fig. 5. For $\Delta = 2$, we find rapid convergence with cluster size to $D \approx 0.56$, consistent with these previous works [27]. For $\Delta < 1$, the "diffusion constant" diverges to a much larger (but still finite) value, consistent with nondiffusive behavior. This diffusive and nondiffusive behavior can be seen in the second two panels. We find that the diffusion constant scales as $\Delta^{-1.5}$ at large Δ. As expected, the two derived diffusion constants differ—by a factor of $\sim$2.1. This is not unexpected: one is averaging over an ensemble of typical states, while the other evolves a single low-energy state. This suggests a temperature dependence of the diffusion constant. Unfortunately, the results are inconclusive at the interesting $\Delta = 1$ point.

B. *XY* spin ladder

It is interesting to analyze different potentially diffusive models under this method. Here, we briefly analyze the *XY* spin ladder for rung widths $\geqslant 2$. This model represents a challenge for the existing methods, as complexity grows much quicker with increasing width and approaches a two-dimensional (2D) limit. This model was chosen to emphasize the lack of dimensional constraints for the method, while retaining 1D behavior. For the spin ladder, the Hamiltonian and symmetric correlator are

$$\hat{H} = \sum_{\langle\alpha\beta ij\rangle} \hat{\sigma}_x^{\alpha i}\hat{\sigma}_x^{\beta j} + \hat{\sigma}_y^{\alpha i}\hat{\sigma}_y^{\beta j}, \tag{9}$$

$$C_X(t) = \frac{1}{N_y}\mathrm{Tr}\left\{\left[\sum_\alpha \hat{\sigma}_z^{\alpha,i}(t)\right]\left[\sum_\beta \hat{\sigma}_z^{\beta,(i+X)\%N}(0)\right]\right\}. \tag{10}$$

Here, α and i index the width and height directions, respectively; the summation averages over each rung of the ladder. This corresponds to spins hopping on a 2D lattice of size $N_y \times N_x$, with N_y finite and $N_x \to \infty$. The results are shown in Fig. 6 for $N_y = 2, 3, 4$ and $N_x \approx 64$ up to cluster size rounding. Curiously, the diffusion value converges almost instantaneously with cluster size to a value of about $D \approx 2.75$. This suggests that there may exist a local hydrodynamic model which describes well the *XY* ladder at infinite temperature.

IV. CONCLUSION

We have applied CTWA to analyze infinite-temperature nonequal time correlation functions in an *XXZ* chain with first- and second-nearest-neighbor interactions, and a variable-width *XY* ladder. We obtained excellent agreement between the results of exact numerical simulations and CTWA predictions for small system sizes. For larger system sizes, where exact diagonalization is not available, we found that CTWA smoothly interpolates between short-time quantum correlations and long-time hydrodynamic correlations. We showed that both the diffusion constant D and the dynamic structure factor converge with the cluster size. Moreover, as our results suggest, D is strongly renormalized by quantum fluctuations and cannot be accurately extracted from either traditional semiclassical approaches (due to their long-time failure) or exact diagonalization (due to limited system sizes).

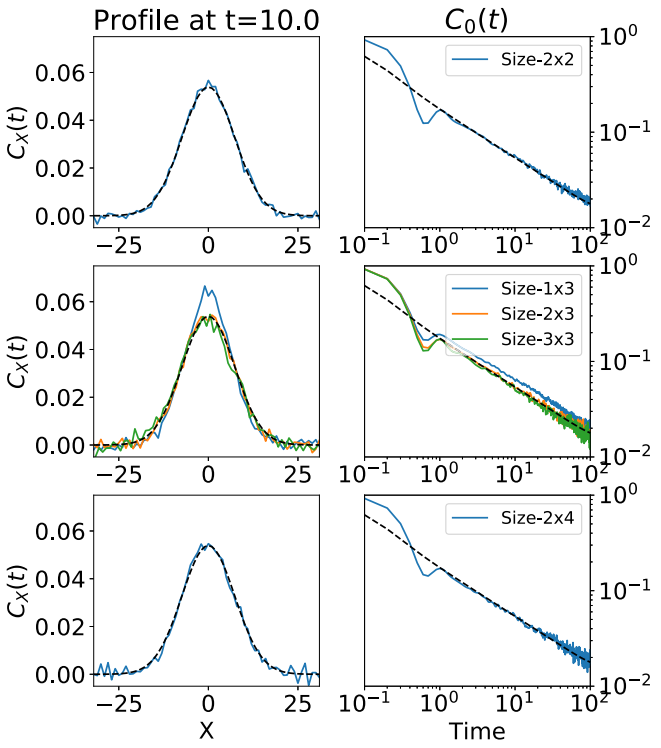

FIG. 6. Behavior of symmetric correlator for an *XY* ladder. Top to bottom are widths of 2, 3, and 4. Left: Gaussian profile at $t = 10$ for different widths. Right: Self-correlator demonstrating diffusive behavior (black dashed line for $D = 2.75$.). Similarly to the next-nearest-neighbor model, there is short-time quantum behavior plus long-time diffusive behavior.

We show that mean-field approaches, where one suppresses quantum fluctuations present in CTWA, give a grossly incorrect prediction for the long-time behavior of the correlation functions and fail to correctly capture diffusion. Similar incorrect hydrodynamic behavior for this model was observed in a matrix-product-state-based TDVP approach due to multiple conservation laws [19,40]. We expect that this failure of the mean-field approaches to correctly recover hydrodynamic behavior is generic and stems from relaxation of the mean-field trajectories for phase space points to nearly time-independent average values.

It is interesting to see how the results of our work can be extended to finite temperatures where both symmetric and antisymmetric correlation functions are nonzero. We anticipate that at least at sufficiently high temperatures, CTWA should remain accurate and allow one to extract both the dissipative and Kubo-type response in strongly correlated regimes. Similarly, extending the model to higher dimensions to capture other coefficients may also be interesting.

ACKNOWLEDGMENTS

We would like to thank E. Altman, F. Pollmann, and D. Sels for stimulating discussions and, additionally, thank F. Pollmann for sharing unpublished results. We would also like to thank the Boston University Shared Computing Cluster for providing computational resources, and the reviewers of this work for their infinite patience. This work was supported by NSF Grant No. DMR-1813499 and AFOSR Grant No. FA9550-16-1-0334.

APPENDIX A: DETAILS OF CTWA

In this Appendix, we summarize key aspects of the cluster truncated Wigner approximation (CTWA), which is used to obtain the results shown in the main text. For further details, we refer to Ref. [21].

The CTWA is a phase space method, which approximately describes unitary dynamics in some Hilbert space via nonlinear Hamiltonian dynamics in some large-dimensional phase space. It consists of four main parts: (1) A definition of phase space, (2) choice of initial conditions, (3) proper classical Hamiltonian equations of motion defining the time evolution of phase space points, and (4) recovering information about observables and correlations. Below we briefly comment on how one implements each part.

(1) In CTWA, phase space is associated with a set of basis operators $G = \{\hat{X}_\alpha\}$ which form a closed Lie algebra: $[\hat{X}_\alpha, \hat{X}_\beta] = i f_{\alpha\beta\gamma} \hat{X}_\gamma \in G$, where $f_{\alpha\beta\gamma}$ are the structure constants. For our system, we choose the set of all operators which span clusters of spins. For example, we can choose all independent strings of products of Pauli matrices $(\hat{\sigma}_x^j,\ \hat{\sigma}_y^j,\ \hat{\sigma}_z^j)$ and the identity, on the sites j which belong to a given cluster. For a cluster consisting of L spins, the total number of independent operators is $\mathcal{D}^2 = 4^L$. All traceless operators are the generators of an $SU(\mathcal{D})$ group with the corresponding structure constants. Operators belonging to different clusters clearly commute with each other. Then the phase space is made by associating this set of operators to phase space variables, $\{\hat{X}_\alpha\} \to \{x_\alpha\}$, satisfying the canonical Poisson bracket relations defined by the same structure constants,

$$\{x_\alpha, x_\beta\} = f_{\alpha\beta\gamma} x_\gamma .$$

In this way, all quantum operators are mapped to functions of phase space variables via Weyl quantization. In particular, any operator belonging to a cluster, which can be represented through a linear combination of the basis operators, maps to a corresponding linear combination of phase space point. The nonlinear operators, e.g., products of basis operators belonging to different clusters, map to equivalent nonlinear functions of phase space points. We note that this construction is a direct generalization of a standard quantum-classical mapping between Pauli matrices and classical spin variables, motivated by ideas of hierarchical mean-field theory [42].

(2) The initial quantum state of the spins is represented by sampling an ensemble of points in phase space weighted by some probability distribution $W(x_\alpha)$, which we call the Wigner function. Although an exact Wigner function exists, we choose a Gaussian function which reproduces the mean and variance of associated basis operators. For example, a Z-polarized state has quantum fluctuations in y: $\langle(\hat{\sigma}_y^{(j)})^2\rangle = 1$ for any site j and likewise for two sites j, j' belonging to the same cluster $\langle(\hat{\sigma}_y^{(j)}\hat{\sigma}_x^{(j')})^2\rangle = 1$. So when drawing initial points, the variables associated with $\hat{\sigma}_y^{(j)}$ and $\hat{\sigma}_y^{(j)}\hat{\sigma}_x^{(j')}$ will be drawn from a Gaussian of variance 1 and mean 0. This can be done in a general manner as detailed in Ref. [21].

Moreover, as discussed in that reference, the actual number of independent operators scales as 2^L, which significantly reduces the complexity of the sampling.

(3) Time evolution is done independently for each point in the ensemble drawn from the Wigner function. It is given by standard classical Hamiltonian equations of motion defined through the Poisson bracket,

$$\frac{\partial x_\alpha(t)}{\partial t} = f_{\alpha\beta\gamma}\frac{\partial H[x(t)]}{\partial x_\beta}x_\gamma(t).$$

Within a cluster, the Hamiltonian is linear and the classical evolution gives exact quantum dynamics. Intercluster interactions lead to a quadratic Hamiltonian and hence to a nonlinear dynamics, which is approximate. As the cluster size increases, the number of nonlinear terms goes down and the CTWA dynamics becomes asymptotically exact.

(4) The expectation values of observables and symmetric correlation functions that we are interested in here are found by averaging corresponding Weyl symbols over the time-evolved phase space points (classical trajectories). In particular,

$$\langle\hat{A}(t)\rangle = \overline{A(\{x(t)\})},$$
$$\langle\{\hat{A}(t),\hat{B}(t')\}_+\rangle = 2\overline{A(\{x(t)\})B(\{x(t')\})},$$

where the overline denotes averaging over the initial conditions drawn from the Gaussian Wigner probability distribution. Note that because the classical equations of motion are generally nonlinear, averaging over the initial conditions and time propagation are noncommuting operations.

Exactness of the single cluster CTWA. In Ref. [21], we mentioned that CTWA exactly reproduces not only expectation values of observables but also their nonequal time correlation functions in the limit when the cluster size becomes equal to the system size and hence the evolution becomes linear. Let us provide here a simple proof of this statement for the symmetric correlation functions. In the linear case, the time evolution of the arbitrary phase space point operator is simply a unitary rotation given by some generally time-dependent unitary matrix $U_{\alpha\beta}(t)$, and therefore both quantum operators and classical phase space points evolve in the same way:

$$\hat{X}_\alpha(t) = \sum_\beta U_{\alpha\beta}(t)\hat{X}_\beta(0), \quad x_\alpha(t) = \sum_\beta U_{\alpha\beta}(t)\hat{x}_\beta(0).$$

For a time-independent Hamiltonian, the unitary is given by the exponent of the effective magnetic torque,

$$U_{\alpha\beta}(t) = e^{M_{\alpha\beta}t}, \quad M_{\alpha\beta} = f_{\alpha\beta\gamma}B_\gamma, \tag{A1}$$

where the magnetic field $\vec{B}$ is defined as usual according to $\hat{H} = -\sum_\alpha B_\alpha\hat{X}_\alpha$. For a time-dependent Hamiltonian, the unitary $U_{\alpha\beta}$ still exists but is defined through a more complicated time-ordered exponential of the time integral of the magnetic field. From this, we find

$$\begin{aligned}\langle\{\hat{X}_\alpha(t),X_\beta(t')\}_+\rangle &= \sum_{\gamma,\delta}U_{\alpha\gamma}(t)U_{\beta\delta}(t')\langle\{\hat{X}_\gamma(0),X_\delta(0)\}\rangle\\ &= \sum_{\gamma,\delta}U_{\alpha\gamma}(t)U_{\beta\delta}(t')\overline{2x_\gamma(0)x_\delta(0)}\\ &= \overline{2x_\alpha(t)x_\beta(t')}.\end{aligned} \tag{A2}$$

Note that even at the level of a single cluster, fluctuations in the initial conditions are crucial for correctly reproducing the nonequal time correlation functions. On the contrary, the mean-field approximation would generally fail to predict such correlation functions. We comment that similar approaches can be used (and have been used in similar contexts [43]) for out of time order correlators (OTOCs), which is a subject of active research.

APPENDIX B: NUMERICAL IMPLEMENTATION DETAILS

Numerics require the implementation of sampling many independent points in phase space from some distribution, then evolving each according to mean-field Hamiltonian equations of motion. To this regard, this is a relatively computationally intensive task: for eight size-8 clusters, there are $8\times4^8 = 524\,288$ phase space variables. However, this is simplified by the particular symmetries of the Gaussian initial conditions and conservation laws, which reduces the number of degrees of freedom to $8\times2^{8+1} = 4096$ complex doubles (see Ref. [21] for details).

Time evolution is then one operator that is constrained to be a product state between clusters with only two nonzero eigenvalues, which is equivalent to the mean-field evolution of a density function, where each cluster sees an effective field from its neighbors. This is implemented via the PYTHON numerical built-in scipy.integrate.complex_ode. For eight size-8 clusters, this requires around 1 second per scale time per sample on a modern hardware core. In order to strongly suppress noise in this work, on the order of 20 000 samples were independently evolved per run, where noise goes as $N_{\text{samples}}^{-1/2}$. In this case, the computational cost is around 500 cpu hours for one run, and is massively parallel. However, on the order of 1000 samples is normally adequate, especially for extensive observables which self-average.

APPENDIX C: SOLUTION OF THE DIFFUSION EQUATION ON A DISCRETE LATTICE

In this Appendix, we detail the derivation of Eq. (6), as well as of the expressions representing the black dashed lines of Figs. 2, 3, 5, and 6. The discrete classical diffusion equation reads

$$\partial_t\rho_i = -D(2\rho_l - \rho_{l-1} - \rho_{l+1}). \tag{C1}$$

Here, ρ represents a conserved charge, which is given by the Z magnetization in our case. This equation can be easily solved in the momentum space using the Fourier transform of ρ,

$$\eta_k = \sum_l e^{ikl}\rho_l, \quad k = 0, 2\pi/N, \ldots, 2\pi(N-1)/N.$$

Then the diffusion equation for each Fourier component η_k reduces to a simple first-order differential equation, which is easy to solve,

$$\begin{aligned}\partial_t\eta_k &= -2D\rho_k[1-\cos(k)]\\ \Rightarrow\ \eta_k(t) &= \eta_k(0)e^{-2Dt[1-\cos(k)]}.\end{aligned} \tag{C2}$$

Using this solution, one can easily find the conformal diffusion width shown in the main text [Eq. (5)]:

$$\begin{aligned} R^2(t) &= \sum_l \frac{N^2}{\pi^2} \sin^2\left(\frac{\pi j}{N}\right)\rho_j(t) \\ &= \sum_{kl} \frac{N^2}{\pi^2} \sin^2\left(\frac{\pi l}{N}\right)e^{-ikl}\eta_k(t) \\ &= \frac{N}{2\pi^2}\left(\eta_0 - \frac{1}{2}\eta_{2\pi/N} - \frac{1}{2}\eta_{-2\pi/N}\right). \end{aligned}$$

Inserting the explicit solution for the form of $\eta_k(t)$ with the initial condition $\eta_k(0) = 1$ and expanding $\cos(2\pi/N) \approx 1 - (2\pi/N)^2/2$ at large N, we derive Eq. (6) from the main text. Similarly, one can find the diffusive structure factor$S(k, \omega)$,

$$S(k,\omega) = \int_{-\infty}^{\infty} dt e^{i\omega t}\eta_k(t) = \frac{4D[1-\cos(k)]}{\omega^2 + 4D^2[1-\cos(k)]^2}. \tag{C3}$$

[1] A. M. Kaufman, M. E. Tai, A. Lukin, M. Rispoli, R. Schittko, P. M. Preiss, and M. Greiner, Quantum thermalization through entanglement in an isolated many-body system, Science **353**, 794 (2016).

[2] C. Neill, P. Roushan, M. Fang, Y. Chen, M. Kolodrubetz, Z. Chen, A. Megrant, R. Barends, B. Campbell, B. Chiaro, A. Dunsworth, E. Jeffrey, J. Kelly, J. Mutus, P. J. O'Malley, C. Quintana, D. Sank, A. Vainsencher, J. Wenner, T. C. White, A. Polkovnikov, and J. M. Martinis, Ergodic dynamics and thermalization in an isolated quantum system, Nat. Phys. **12**, 1037 (2016).

[3] C. Gogolin and J. Eisert, Equilibration, thermalisation, and the emergence of statistical mechanics in closed quantum systems, Rep. Prog. Phys. **79**, 056001 (2016).

[4] F. Borgonovi, F. Izrailev, L. Santos, and V. Zelevinsky, Quantum chaos and thermalization in isolated systems of interacting particles, Phys. Rep. **626**, 1 (2016).

[5] L. F. Santos and M. Rigol, Onset of quantum chaos in one-dimensional bosonic and fermionic systems and its relation to thermalization, Phys. Rev. E **81**, 036206 (2010).

[6] A. Polkovnikov, K. Sengupta, A. Silva, and M. Vengalattore, Colloquium: Nonequilibrium dynamics of closed interacting quantum systems, Rev. Mod. Phys. **83**, 863 (2011).

[7] L. D'Alessio, Y. Kafri, A. Polkovnikov, and M. Rigol, From quantum chaos and eigenstate thermalization to statistical mechanics and thermodynamics, Adv. Phys. **65**, 239 (2016).

[8] S. Mukerjee, V. Oganesyan, and D. Huse, Statistical theory of transport by strongly interacting lattice fermions, Phys. Rev. B **73**, 035113 (2006).

[9] R. Steinigeweg, F. Heidrich-Meisner, J. Gemmer, K. Michielsen, and H. De Raedt, Scaling of diffusion constants in the spin-$\frac{1}{2}$ xx ladder, Phys. Rev. B **90**, 094417 (2014).

[10] K. Agarwal, S. Gopalakrishnan, M. Knap, M. Müller, and E. Demler, Anomalous Diffusion and Griffiths Effects Near the Many-Body Localization Transition, Phys. Rev. Lett. **114**, 160401 (2015).

[11] J. Richter, F. Jin, H. De Raedt, K. Michielsen, J. Gemmer, and R. Steinigeweg, Real-time dynamics of typical and untypical states in nonintegrable systems, Phys. Rev. B **97**, 174430 (2018).

[12] M. Moeckel and S. Kehrein, Interaction Quench in the Hubbard Model, Phys. Rev. Lett. **100**, 175702 (2008).

[13] J. Lux, J. Müller, A. Mitra, and A. Rosch, Hydrodynamic long-time tails after a quantum quench, Phys. Rev. A **89**, 053608 (2014).

[14] M. Ljubotina, M. Znidaric, and T. Prosen, Spin diffusion from an inhomogeneous quench in an integrable system, Nat. Commun. **8**, 16117 (2017).

[15] J. De Nardis, D. Bernard, and B. Doyon, Diffusion in generalized hydrodynamics and quasiparticle scattering, Sci. Post. Phys. **6**, 49 (2019).

[16] Y. Ashida, T. Shi, M. C. Bañuls, J. I. Cirac, and E. Demler, Variational principle for quantum impurity systems in and out of equilibrium: Application to Kondo problems, Phys. Rev. B **98**, 024103 (2018).

[17] D. Gobert, C. Kollath, U. Schollwöck, and G. Schütz, Real-time dynamics in spin-$\frac{1}{2}$ chains with adaptive time-dependent density matrix renormalization group, Phys. Rev. E **71**, 036102 (2005).

[18] P. Kramer, A review of the time-dependent variational principle, J. Phys. Conf. Ser. **99**, 012009 (2008).

[19] E. Leviatan, F. Pollmann, J. H. Bardarson, D. A. Huse, and E. Altman, Quantum thermalization dynamics with matrix-product states, arXiv:1702.08894.

[20] B. Kloss, Y. B. Lev, and D. Reichman, Time-dependent variational principle in matrix-product state manifolds: Pitfalls and potential, Phys. Rev. B **97**, 024307 (2018).

[21] J. Wurtz, A. Polkovnikov, and D. Sels, Cluster truncated Wigner approximation in strongly interacting systems, Ann. Phys. **395**, 341 (2018).

[22] L. Landau and E. Lifshitz, *Statistical Physics*, Vol. 5 (Elsevier Science, New York, 2013).

[23] L. Onsager, Reciprocal relations in irreversible processes. I., Phys. Rev. **37**, 405 (1931).

[24] P. A. M. Dirac, Note on exchange phenomena in the Thomas atom, Math. Proc. Cambridge Philos. Soc. **26**, 376 (1930).

[25] H.-D. Meyer, U. Manthe, and L. Cederbaum, The multi-configurational time-dependent Hartree approach, Chem. Phys. Lett. **165**, 73 (1990).

[26] T. Prosen, Open *XXZ* Spin Chain: Nonequilibrium Steady State and a Strict Bound on Ballistic Transport, Phys. Rev. Lett. **106**, 217206 (2011).

[27] C. Karrasch, J. E. Moore, and F. Heidrich-Meisner, Real-time and real-space spin and energy dynamics in one-dimensional spin-$\frac{1}{2}$ systems induced by local quantum quenches at finite temperatures, Phys. Rev. B **89**, 075139 (2014).

[28] J. De Nardis, D. Bernard, and B. Doyon, Hydrodynamic Diffusion in Integrable Systems, Phys. Rev. Lett. **121**, 160603 (2018).

[29] P. Blakie, A. Bradley, M. Davis, R. Ballagh, and C. Gardiner, Dynamics and statistical mechanics of ultra-cold Bose gases using c-field techniques, Adv. Phys. **57**, 363 (2008).

[30] R. Steinigeweg and W. Brenig, Spin Transport in the *XXZ* Chain at Finite Temperature and Momentum, Phys. Rev. Lett. **107**, 250602 (2011).

[31] D. J. Luitz and Y. B. Lev, The ergodic side of the many-body localization transition, Ann. Phys. **529**, 1600350 (2017).

[32] Y. Bar Lev, G. Cohen, and D. R. Reichman, Absence of Diffusion in an Interacting System of Spinless Fermions on a One-Dimensional Disordered Lattice, Phys. Rev. Lett. **114**, 100601 (2015).

[33] V. Oganesyan, A. Pal, and D. A. Huse, Energy transport in disordered classical spin chains, Phys. Rev. B **80**, 115104 (2009).

[34] A. Das, S. Chakrabarty, A. Dhar, A. Kundu, D. A. Huse, R. Moessner, S. S. Ray, and S. Bhattacharjee, Light-Cone Spreading of Perturbations and the Butterfly Effect in a Classical Spin Chain, Phys. Rev. Lett. **121**, 024101 (2018).

[35] S. Sachdev, *Quantum Phase Transitions*, 2nd ed. (Cambridge University Press, Cambridge, 2011).

[36] D. J. Luitz and Y. Bar Lev, Anomalous Thermalization in Ergodic Systems, Phys. Rev. Lett. **117**, 170404 (2016).

[37] J. T. Edwards and D. J. Thouless, Numerical studies of localization in disordered systems, J. Phys. C: Solid State Phys. **5**, 807 (1972).

[38] M. Gaudin, in *The Bethe Wavefunction*, edited by J.-S. T. Caux (Cambridge University Press, Cambridge, 2014).

[39] T. Prosen, Exact Nonequilibrium Steady State of a Strongly Driven Open *XXZ* Chain, Phys. Rev. Lett. **107**, 137201 (2011).

[40] S. Gopalakrishnan, R. Vasseur, and B. Ware, Anomalous relaxation and the high-temperature structure factor of *XXZ* spin chains, Proc. Natl. Acad. Sci. **116**, 16250 (2019).

[41] S. Gopalakrishnan and R. Vasseur, Kinetic Theory of Spin Diffusion and Superdiffusion in *XXZ* Spin Chains, Phys. Rev. Lett. **122**, 127202 (2019).

[42] C. D. Batista and G. Ortiz, Algebraic approach to interacting quantum systems, Adv. Phys. **53**, 1 (2004).

[43] M. Schmitt, D. Sels, S. Kehrein, and A. Polkovnikov, Semiclassical echo dynamics in the Sachdev-Ye-Kitaev model, Phys. Rev. B **99**, 134301 (2019).